where

$$\lambda = \dot{w}_t T_e / P_c = f \text{ (axial chamber gas velocity)} \quad (16)$$

$$C_f = C_{fo} + \partial C_f/\partial P_{nt}(P_{nt} - P_{nto}) + \partial C_f/\partial Rm(Rm - Rm_o) + \partial C_f/\partial A_t(A_t - A_{to}) \quad (17)$$

Fourteen variables [assuming Eq. (14) has seven terms] are involved. These are: C_1–C_7 in Eq. (14); $C_8 = \beta_o$, $C_9 = \partial\beta/\partial\lambda$, and $C_{10} = \partial\beta/\partial A_t$ in Eq. (15); and $C_{11} = C_{fo}$, $C_{12} = \partial C_f/\partial P_{nt}$, $C_{13} = \partial C_f/\partial Rm$, and $C_{14} = \partial C_f/\partial A_t$ in Eq. (17).

Values for β_o and C_{fo} (at the rated point, no erosion) are chosen to correspond to values of λ_o, A_{to}, P_{nto}, and Rm_o. It is recommended that these relationships be established in the following order: A_{to} = noneroded throat area; λ_o = chamber velocity function evaluated at the full thrust position with A_{to}; $\beta_o = P_{nto}/P_o$ at λ_o and A_{to}; and C_{fo} = thrust coefficient at P_{nto}, A_{to}, and Rm_o. It is then assumed that all of the undetermined partial derivatives are constants. Equation (13) is rearranged, squared, and summed over the entire test duration (i.e., data slice, by slice) to obtain the error function Ψ;

$$\Psi = \frac{1}{N}\sum_{i=1}^{N}\left(\frac{P_c}{F}\beta A_t C_f - 1\right)_i^2 \quad (18)$$

where N = number of data slices.

The problem of minimizing Eq. (18) readily lends itself to a digital computer solution. Initial values for C_1–C_7 are determined by assuming a C^* for each data slice during the test duration, then estimating A_t. Data from similar past tests are very useful at this point in order to initialize C_1–C_7 more accurately by a least-squares (usually 6th degree or larger) fit of the "first cut" $A_t(t)$ data. Coefficients C_8–C_{14} can be initialized from theoretical considerations, past test data, or engineering judgment. The most important aspect in initializing C_9–C_{14} is determining the correct order of magnitude and sign.

The task of minimizing Eq. (18) becomes that of setting all the first partial derivatives equal to zero. Initially the steepest rate of descent method was used with the first and second partial derivatives being computed numerically. The particular independent variable possessing the second partial derivative of highest absolute magnitude was perturbed in an effort to set its first partial derivative to zero. The remaining variables were held constant, i.e.,

$$\Delta C_i = (0 - \partial\Psi/\partial C_i)/(\partial^2\Psi/\partial C_i^2) \quad (19)$$

where Ψ = error function (18).

This process was repeated in a recursive manner until the numerical values of all of the first partial derivatives were approximately zero. This method proved cumbersome in that it completely ignored the off-diagonal terms of the second partial derivative matrix. Convergence was improved when these off-diagonal terms were taken into account. A second algorithm employed was only limited by the errors associated with the numerical calculation of the first and second partial derivatives;

$$[\Delta C_j] = [\partial^2\Psi/\partial C_{ij}^2]^{-1}\cdot[0 - \partial\Psi/\partial C_i], \quad i = 1, \ldots, 14; \quad j = 1, \ldots, 14 \quad (20)$$

It was impossible to set the first partial derivatives exactly to zero; however, values in the order of 0.001 (nondimensionalized) were obtained.

A breakthrough on this method was realized when more elaborate optimization algorithms were employed such as those contained in SLANG,** a TRW Systems engineering modeling language for system simulation and optimization. SLANG has the advantage that, as part of its compiler functions, it automatically programs the first and second partial derivatives from the original function (in this case, Ψ). This eliminated the errors inherent in numerical calculation of partial derivatives. Secondly, SLANG employs more elaborate optimization algorithms with various safeguards for purposes of maintaining the solution continuity and preventing "blow-ups." The time required to minimize Ψ was reduced by a factor of 10, and the magnitude of Ψ was reduced by a factor of 20, as compared to the former methods.

** SLANG™, copyright, 1968, TRW Inc., Redondo Beach, Calif.

Low-Thrust, Constant-Acceleration Trajectories for Solar Probe Missions

HARVEY T. BROCK JR.*
U.S. Air Force Academy, Colo.
AND
ROGER W. JOHNSON†
Air Force Institute of Technology, Wright-Patterson Air Force Base, Ohio

THE purpose of this investigation is to determine the feasibility of using tangential thrust, constant-acceleration trajectories for close solar probe missions. Trajectories to 0.05 a.u. using low-thrust electric engines are considered. Both HEV = 0 and HEV > 0 (hyperbolic excess velocities) after escape from the earth by chemical rocket are considered. Previous investigators of solar probe missions have considered constant-thrust trajectories with or without coast phases,[1-2] but, as far as we are able to determine, no reports on constant-acceleration trajectories for solar probe missions are in the open literature.

Several criteria are used to judge the usefulness of the various trajectories investigated. One of these is the total time T required for the probe to reach a point 0.05 a.u. from the sun. Current and projected electric-engine lifetimes are of the order of 10,000 hr (416 days).[3] An upper limit of 400 days is chosen for the time to reach the desired location. Another consideration is the total velocity change (decrease, ΔV) to be accomplished during the flight. The third criterion is the terminal angle ϕ between the sun-earth radius and the sun-probe radius. This angle should be 90° in order to have the best possible radio communication with the probe when it reaches 0.05 a.u. The initial assumptions are: 1) initially, boost to escape velocity is by a chemical

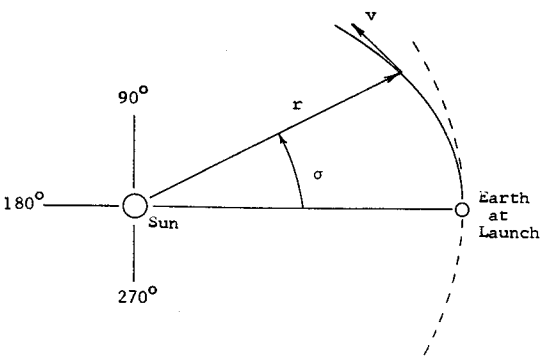

Fig. 1 Heliocentric-ecliptic coordinate system.

Received October 7, 1968; revision received September 12, 1969.

* Captain, U.S. Air Force, Instructor of Astronautics.

† Lt. Colonel, U.S. Air Force, Associate Professor of Electrical Engineering.

Table 1 Summary of data on constant-acceleration trajectories

HEV	a_t, $10^{-4}g_e$	T, days	ΔV, 10^3fps	ϕ, deg	Payload ratio $\alpha_s = 0.1$	Payload ratio $\alpha_s = 0.2$
0	2.2–2.5	172.2–222	119.7–142.7	36–56	0.082–0.112	0.246–0.281
	3.4–4	102.5–105.9	100–114	43–115	0.031–0.084	0.175–0.247
$0.05V_{c0}$	2.2–2.4	207.3–214.6	131–138.1	42.5–58.2	0.089–0.120	0.253–0.289
	3.4–4	98.4–101	95.2–109.3	42–106.5	0.033–0.094	0.185–0.260
$0.10V_{c0}$	2.1–2.3	204.8–212.2	124–130.8	47.2–62.8	0.110–0.143	0.277–0.314
	3.4–4	94.8–96.6	90.6–105.5	36.1–91.4	0.043–0.105	0.194–0.272
$0.15V_{c0}$	2–2.2	203.1–210.5	117–123.8	48–65	0.134–0.168	0.304–0.339
	3.4–4	91.7–92.8	87.6–101.9	31.5–78	0.043–0.111	0.206–0.279

booster, 2) escape occurs at the limit of the earth's sphere of influence, 3) the earth's gravitational attraction can be neglected during the probe's heliocentric trajectory, 4) the sun is a point mass during all phases of the probe's trajectory and is the only body affecting its motion, 5) all motion takes place in the plane of the ecliptic, 6) the orbit of the earth is circular with a radius of 1 a.u., 7) the earth's mean daily motion is 0.985 deg/day, and 8) solar radiation pressure effects are negligible.

The equations of motion are written in a heliocentric-ecliptic coordinate system using polar coordinates r and σ (see Fig. 1). The general form of the state differential equations which are integrated numerically is $\mathbf{x}' = \mathbf{f}(\mathbf{x},\mathbf{u})$, or, in component form

$$r' = w/r_0, \quad t' = r/r_0 \tag{1}$$

$$v' = -(k^2w/r^2vr_0) + (ra_t/r_0) \tag{2}$$

$$w' = (v^2r/r_0) - (k^2/r_0) - (wra_t/vr_0) \tag{3}$$

$$\sigma' = [v^2 - (w/r)^2]^{1/2}/r_0 \tag{4}$$

where v,w = velocity components, $w = \mathbf{v}\cdot\mathbf{r}$, $k^2 = Gm_{sun}$, a_t = tangential acceleration magnitude, and (′) indicates differentiation with respect to an auxiliary variable τ. A unique feature of Eqs. (1–4) is the use of $t' = r/r_0$ as a means of obtaining a variable time step in the numerical integration scheme. The acceleration vector was always maintained tangent to the path of the probe.

Initial conditions for the probe's heliocentric trajectory, based on the assumptions noted previously, are $r_0 = 1$ a.u., v_0 = circular velocity at 1 a.u., and $r_0 = \sigma_0 = t_0 = 0$. Values of tangential acceleration in the range $2 \times 10^{-4}g_e \leq a_t \leq 7 \times 10^{-4}g_e$ are used; this range represents approximately the limits of acceleration possible using electric engine propulsion.[4]

Equations (1–4) are solved using a modified predictor-corrector method developed by Hamming.[5] It is necessary to maintain a constant-integration step size when using Hamming's equations. By the use of $t' = r/r_0$, a constant integration step size $\Delta\tau$ is maintained while the physical time step Δt varies with the value of r. By using this additional equation and integrating with respect to τ, it is possible to obtain a higher accuracy and achieve a more stable numerical integration. The computer programs for these calculations are written in FORTRAN IV.

Constant-Acceleration Trajectories with HEV = 0 at Injection into Heliocentric Orbit

Figure 2 illustrates two of the trajectories obtained; a_t affects the number of revolutions the probe makes prior to reaching 0.05 a.u. Figure 3 shows the total time required for the probe to reach a point 0.05 a.u. from the sun for the range of a_t investigated. The third column of Table 1 shows

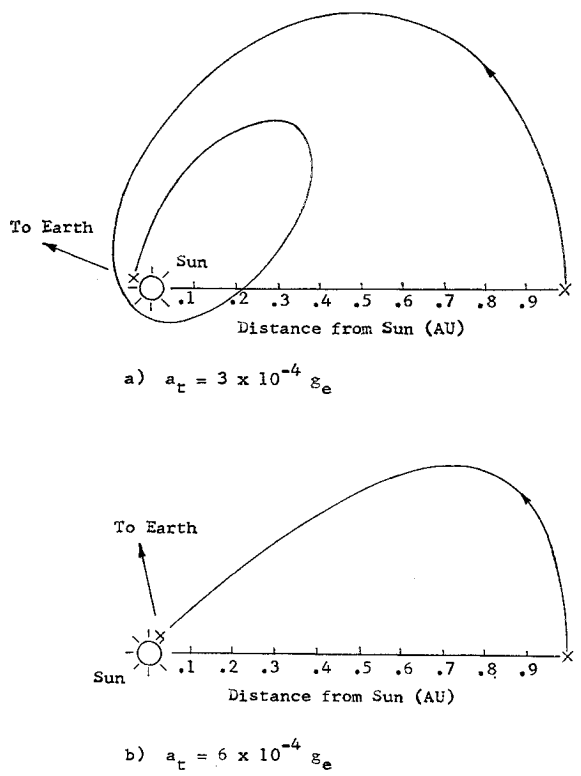

Fig. 2 Typical solar probe trajectories with constant tangential acceleration.

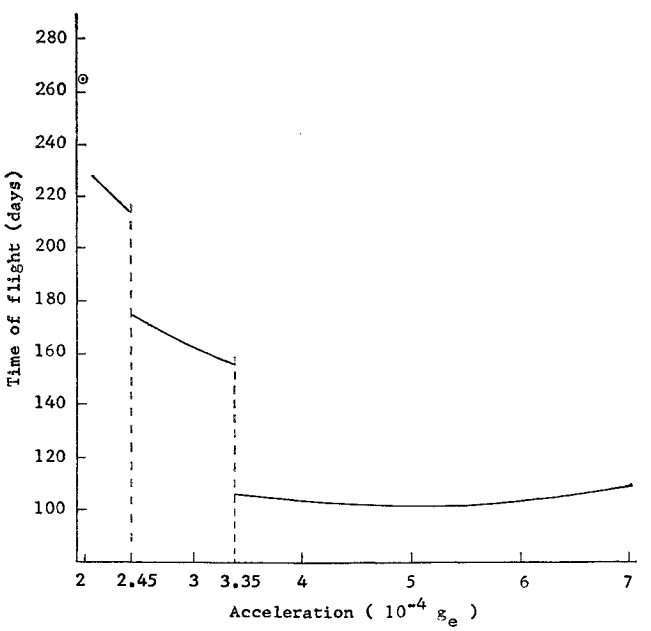

Fig. 3 Total time required for probe to reach a point 0.05 a.u. from the sun.

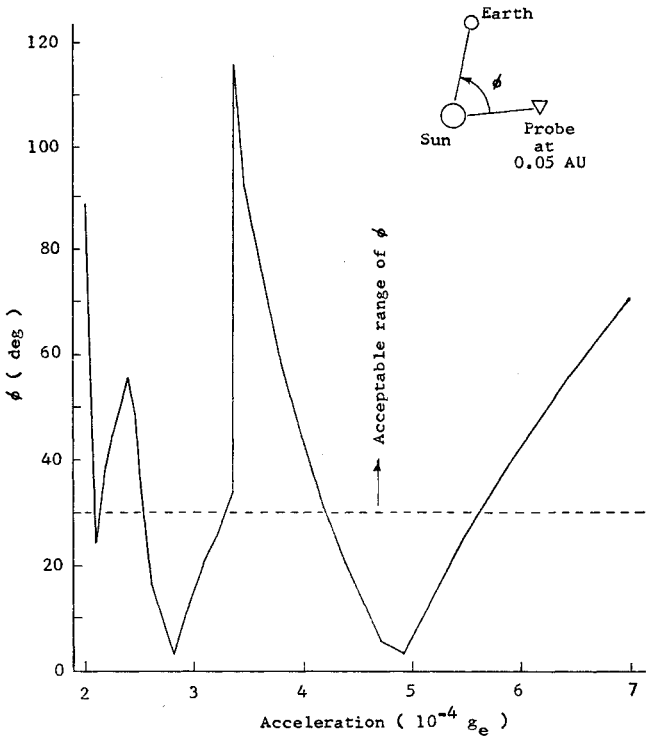

Fig. 4 Variation of terminal configuration angle with acceleration.

the ΔV of the probe due solely to the thrustor ($\Delta V = a_t T$, where T is the total time of flight, since a_t remains constant). This ΔV is negative since the thrustor is assumed to act in the opposite direction to the probe's velocity at all times. The terminal configuration angle ϕ illustrated in Fig. 4 should be 90° for ideal communication between the probe and earth. The acceptable range of angles is taken to be $30° < \phi < 150°$. From Fig. 4, it is evident that only three bands of a_t (in $10^{-4}g_e$) have terminal angles within these limits, namely: 2.2–2.5, 3.3–4.2, and 5.7–7.0. The final measure of the usefulness of the trajectories investigated is the payload ratio available for the probe. The payload ratio for a constant-acceleration vehicle is given by Stuhlinger.[4] Figure 5 presents the payload ratios calculated for the various acceleration values.

Based on the investigation of trajectories with HEV = 0 at injection into heliocentric orbit, it is concluded that there are two ranges of a_t (in $10^{-4}g_e$) which would be useful for solar probe missions to 0.05 a.u.: 3.4–4.0, and 2.2–2.5. Table 1 summarizes the data associated with each range of acceleration values.

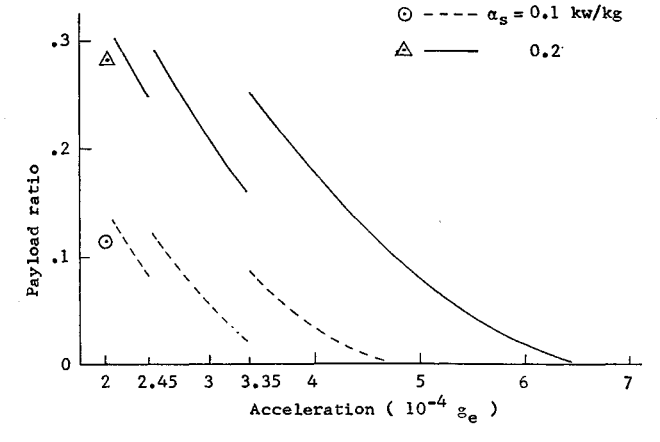

Fig. 5 Variation of payload ratio with specific power (a_s) and acceleration.

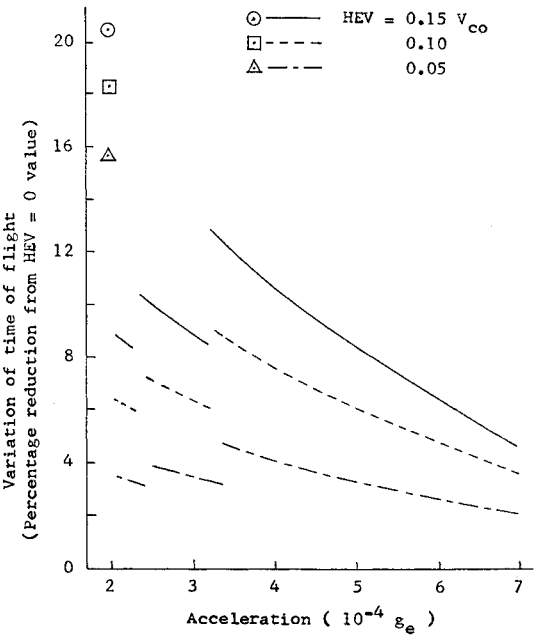

Fig. 6 Effect of HEV > 0 on total time of flight.

Constant-Acceleration Trajectories with HEV > 0 at Injection into Heliocentric Orbit

The initial velocities of the probe considered are 0.85 V_{c0}, 0.90 V_{c0}, and 0.95 V_{c0}, corresponding to tangential HEV's of 0.15 V_{c0} (14,655 fps), 0.10 V_{c0} (9770 fps), and 0.05 V_{c0} (4885 fps), respectively. In order to obtain an HEV > 0, it is necessary to reduce the total mass of the probe injected into heliocentric orbit by a chemical booster because of the extra fuel required to be carried. The corresponding burnout velocities (based on v_{escape} = 36,200 ft/sec at 8000 naut. mile altitude) are 39,100, 37,550, and 36,600 fps, respectively. The effect of an HEV > 0 on T is illustrated in Fig. 6. Again, as in the HEV = 0 investigation, the terminal configuration angle is the major limiting factor in determining which trajectories are feasible for the solar probe mission. No significant increase in the range of accelerations is obtained for any of the HEV > 0 cases. The major effect on the range of possible accelerations is a downward shift of the acceleration ranges as indicated in Table 1. Figure 7 illustrates the increase in payload ratio obtained from HEV = 0.15 V_{c0} case. Curves are presented only for the useful ranges of acceleration as determined by the terminal configuration angle results. The HEV = 0.05 V_{c0} and HEV = 0.10 V_{c0} curves lie between the two curves shown. The payload ratios are also presented in Table 1 for each of the cases considered.

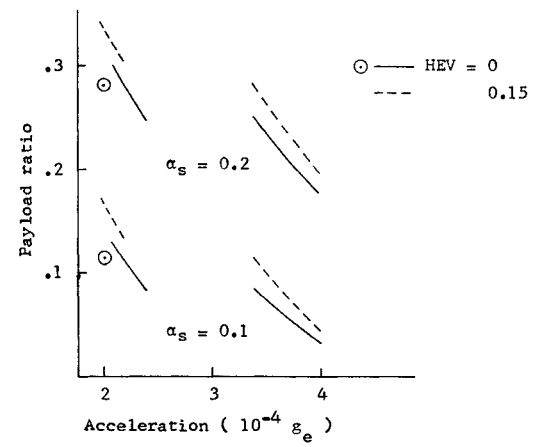

Fig. 7 Effect of HEV > 0 on payload ratio.

Only very narrow ranges of acceleration are feasible for solar probe missions with HEV > 0 at launch into heliocentric orbit. There are increases in payload ratios obtainable by using these trajectories as compared to the HEV = 0 cases. However, the tradeoff in total mass injected initially into orbit about the sun for the additional burnout velocity required may not make the HEV > 0 cases desirable for solar probe missions.

Conclusions

Relatively simple low-thrust, constant-acceleration trajectories are useful for solar probe missions for only a very limited range of accelerations. The major limiting factor is the terminal configuration angle ϕ. All trajectories studied met the success criteria for total time and velocity to be gained.

References

[1] Strack, W. C., "Solar Electric Propulsion System Performance for the 0.1-a.u. Solar Probe Mission," TM-X-52201, 1966, NASA.

[2] Strack, W. C., "Combined High-Low Thrust Propulsion for the Close Solar Probe Mission," TN-D-3145, 1965, NASA.

[3] Mickelsen, W. R., "Auxiliary and Primary Electric Propulsion, Present and Future," *Journal of Spacecraft and Rockets*, Vol. 4, No. 11, Nov. 1967, pp. 1409–1423.

[4] Stuhlinger, E., *Ion Propulsion for Space Flight*, McGraw-Hill, New York, 1964, Chap. 4.

[5] Hamming, R. W., "Stable Predictor-Corrector Methods for Ordinary Differential Equations," *Journal of the Association of Computing Machinery*, Vol. 6, 1959, pp. 37–47.

Surface Roughness Effects on Radiant Heat Transfer

R. G. Hering* and T. F. Smith†
University of Illinois at Urbana-Champaign, Urbana, Ill.

THE apparent thermal radiation properties of a one-dimensionally rough surface with V-shaped roughness elements of identical included angle were recently reported.[1] In this Note the rough-surface properties are employed to examine the influence of surface roughness on the radiant energy transfer rate of an isolated plane surface with specified uniform temperature when the surface is fully illuminated by a uniform collimated solar flux. Surface roughness effects on equilibrium temperature were explored in a recent study.[2]

The radiant heat-transfer rate per unit area from the isolated rough surface q with apparent emittance ϵ_H and direction-dependent, apparent solar absorptance $\alpha_a^*(\theta')$ in the solar field of solar constant S is determined by the difference between the emission rate and the rate of absorption of incident energy. For a surface at temperature T, the radiant heat-transfer rate per unit black surface emissive power is

$$q/\sigma T^4 = \epsilon_H - \alpha_a^*(\theta')S^* \cos\theta' \qquad (1)$$

where σ and θ' denote the Stefan-Boltzmann constant and the direction of incident flux relative to the normal of the mean surface plane, respectively, and $S^*(= S/\sigma T^4)$ is a dimensionless energy ratio characterizing the relative magnitude of solar flux to surface emission rate. For a smooth surface of identical material, the apparent properties are replaced with wall emittance ϵ_w and wall absorptance for solar energy α_w^* both of which are taken direction independent.

The apparent properties depend on groove wall properties (ϵ_w, α_w^*), roughness element included angle (χ), and parameters which characterize interreflection phenomena within surface asperities. The latter are the wall specularity for emission $(\rho_s/\rho)_w$ and the wall specularity for solar energy $(\rho_s^*/\rho^*)_w$, where ρ_s (or ρ_s^*) and ρ (or ρ^*) denote the specular component of wall reflectance and total reflectance, respectively. As $(\rho_s/\rho)_w$ [or $(\rho_s^*/\rho^*)_w$] varies from zero to unity, the groove walls change from diffusely reflecting to specularly reflecting. Typical apparent property results are presented in Ref. 1.

Typical dimensionless heat-transfer results for $\chi = 45°$ are presented for wall property values of 0.1 and 0.9 and the extreme values of the specularity parameters in Figs. 1, 2, and 3 for S^* values of 0.1, 1.0, and 10, respectively. The smooth- and rough-surface heat fluxes are influenced in a similar manner by wall properties, energy ratio S^*, and di-

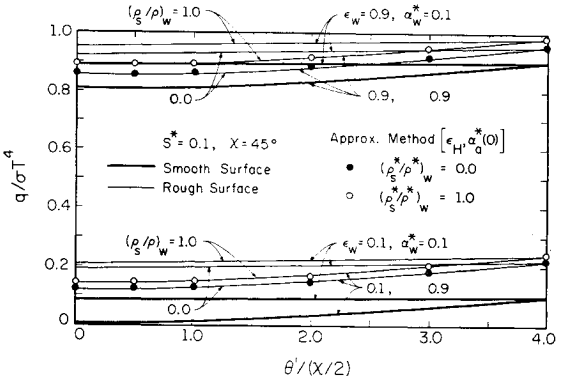

Fig. 1 Surface roughness effects on radiant heat transfer ($S^* = 0.1$).

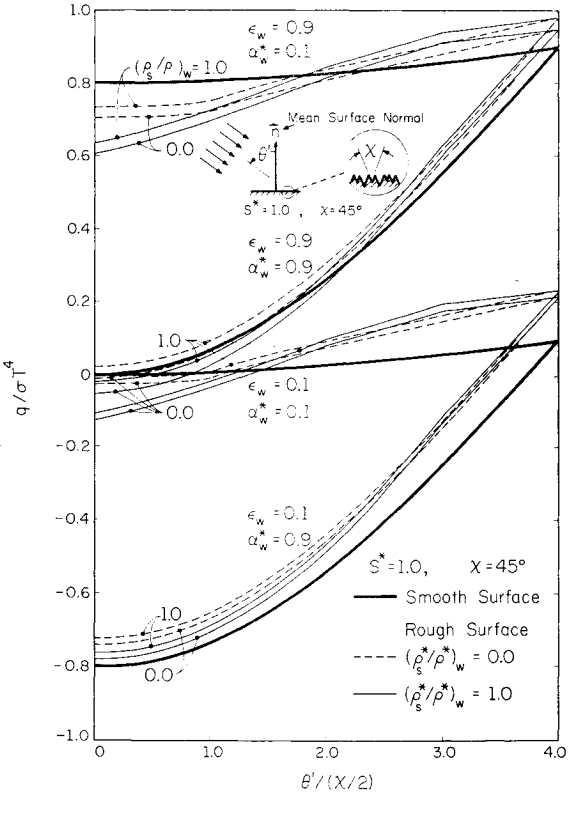

Fig. 2 Surface roughness effects on radiant heat transfer ($S^* = 1.0$).

Received September 15, 1969.

* Professor, Department of Mechanical Engineering. Member AIAA.

† Research Assistant, Department of Mechanical Engineering.